Joint migration inversion: Simultaneous determination of velocity fields and depth images using all orders of scattering

D. J. Verschuur[1], X. R. Staal[1], and A. J. Berkhout[1]

Abstract

The future in seismic exploration and seismic monitoring is the inclusion of all orders of scattering in the imaging and inversion algorithms. Using the full wavefield in an inversion process allows us to surpass imprints provided by incomplete acquisition and provide more accurate information on the subsurface, as noise becomes signal. We describe an inversion process that does not use the standard parameters from finite-difference-type modeling (being local velocity and density) but that describes the seismic data in terms of elastic reflectivity operators and propagation operators. With these operators, our full-wavefield modeling process builds the complete two-way seismic response. A major advantage of our alternative to the traditional full-waveform inversion methodology is that reflectivity operators are traveltime-free and propagation operators are scattering-free, making the inversion problem significantly more linear. A major advantage of our algorithm is (1) that multiples are utilized to improve both image and velocity accuracy, and (2) that both image and velocities are utilized to make a contribution in the nonlinear migration process. Hence, in joint migration inversion, multiples have a twofold active role.

Introduction

To meet the challenges of imaging in difficult areas or to get more accurate reservoir information, we need to get more detailed velocities, and we have to include as well as make use of all complex propagation and reflection phenomena in our seismic data. This means that the era of traditional linear imaging methods will end.

The most well-known proposal to estimate detailed velocities from seismic data is so-called full-waveform inversion (FWI) (Tarantola, 1984), which attempts to fit the measured data based on full-waveform modeling methods. As discussed by Symes (2008) and Virieux and Operto (2009), the objective function of Tarantola's inversion approach has many local minima. This problem can be partly solved when FWI is applied to diving waves and/or to low-frequency data (Operto et al., 2004; Plessix et al., 2010). However, because of the involved finite-difference modeling, the method is computationally very expensive, and it requires very long offsets to have enough depth penetration as well as very low frequencies to avoid the necessity of accurate starting models. Actually, the current practice of diving-wave inversion cannot always be called "full-waveform inversion" as overall amplitude information and multiples are often neglected. Next, in common workflows its output — being a velocity model — will be used in a primary depth-migration process. This strict division of nonlinear velocity estimation and linear imaging is most unfortunate as the limitations of current imaging algorithms — like improper handling of multiples and transmission effects — will be imprinted in the final result.

Primary reflection energy traditionally has been the input for imaging and migration velocity analysis, initially based on kinematic behavior via image-gather analysis (Stork, 1992). To automate velocity estimation and take into account the wave character of reflection energy, wave-equation migration velocity analysis (WEMVA) (Sava and Biondi, 2004) attempts to optimize the imaging condition in depth migration iteratively. The method is very suitable for finding a smooth macro-velocity model (Symes, 2008) and can handle much more complexity in the subsurface compared to kinematic-based algorithms. A fundamental shortcoming of all these approaches is that they are based on primary reflection energy.

Recently, we have seen proposals to combine WEMVA and FWI into a joint inversion scheme by Fleury and Perrone (2012), Zhou et al. (2012), and Biondi and Almomin (2013). Alternatively, the FWI scheme is adapted to include reflection energy as well, but this leads to the problem of mixing of reflection and propagation effects in one inversion parameter (the velocity field), making the inversion highly nonlinear. To reduce this nonlinearity, during the FWI process wavefields can be separated in up- and downgoing components, providing different gradients that can be filtered (Wang et al., 2013), or the velocity field is separated in a low-frequency part (the background) and a high-frequency part (the perturbation), again calculating different gradients for each part (see, e.g., Wu and Alkhalifah, 2015). This yields valuable improvements, but common practice is that such FWI methods provide a detailed velocity model that will be the input for a separate linear depth migration algorithm that cannot fully profit from this rich velocity information. In addition, reflection in the earth is not generated by P-wave velocity contrasts only. Densities and S-wave velocities will need to be incorporated in full-bandwidth, anisotropic 3D FWI before it can accurately represent the seismic reflection data (Krebs et al., 2016).

Therefore, a logical next step is to integrate velocity estimation and migration in one consistent process that is able to handle complex wave propagation and that provides an artifact-free, high-resolution image. First attempts in this direction were taken more than 20 year ago in the so-called migration-based traveltime tomography (MBTT) (Clément and Chavent, 1993; Chavent et al., 1994), where the forward modeling of seismic data is described in independent propagation-based and reflection unknowns, and, by means of Born-type demigration, the observed data could be mimicked. In this way, the nonlinear inversion method of primary reflections becomes more linear.

With a similar thinking, joint migration inversion (JMI), which focuses on the full-bandwidth, multiorder reflection response, was introduced (Berkhout, 2012; Staal and Verschuur, 2012; Berkhout, 2014c). Within JMI, propagation and reflection are described by two independent sets of operators, while together they are used in a two-way modeling scheme (full-wavefield modeling, or FWMod) that models the seismic reflection response including all of its complex, higher-order scattering effects. One

[1]Delft University of Technology.

http://dx.doi.org/10.1190/tle35121037.1.

unique feature of JMI is that its output consists of both a migration velocity model and a high-resolution image, in which multiples and transmission effects are fully accounted for. A second feature is that the reflectivity operators are angle-dependent and contain the *elastic* PP reflectivity effects. Thirdly, in a similar fashion, wave propagation operators can be defined such that they contain anisotropic propagation effects (Alshuhail et al., 2014). Finally, as the full-wavefield modeling process continuously updates the up/downgoing wavefields at each depth level, multiples can play an active role in imaging and velocity updating.

In this contribution to this FWI special section, we show our latest experience regarding the features of the JMI process and demonstrate that it is an integrated alternative for the two-step workflow of (1) nonlinear FWI followed by (2) linear migration.

Review of joint migration inversion

The backbone of the JMI process is the forward-modeling engine, called full-wavefield modeling. In the end, the aim of JMI is to match our forward-modeled data with the observed data. Therefore, JMI can be called a full-waveform inversion process. On the other hand, the inversion parameters in JMI are basically the imaging parameters, being reflectivity and propagation operators. Therefore, JMI can also be considered as an extended form of least-squares imaging (Nemeth et al., 1999) that includes all angle-dependent and multiple scattering, transmission effects, and, in addition, embeds automatic velocity updating.

In FWMod, the up/downgoing wavefields are calculated at a fine set of depth levels $z_n, n = 0,\ldots,M$, separated by a small distance Δz. Scattering is assumed to take place at these depth levels, via upward and downward scattering operators $\mathbf{R}^{\cup}(z_n, z_n)$ and $\mathbf{R}^{\cap}(z_n, z_n)$, respectively; in between these levels, the wavefields

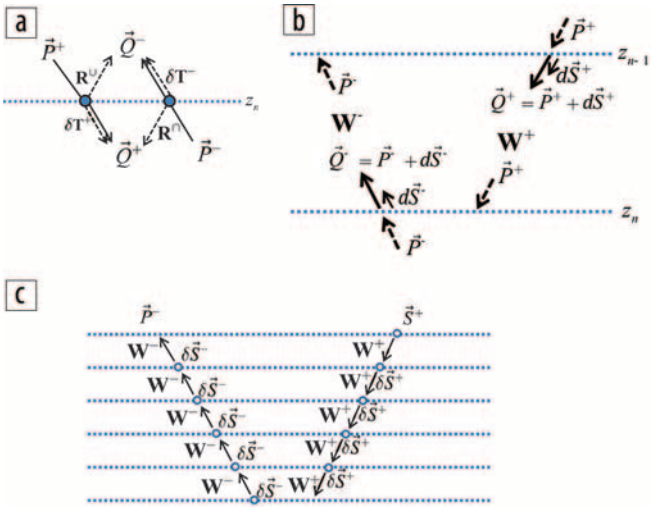

Figure 1. (a) Wavefield relationships and scattering operators at each gridpoint in the subsurface. The incoming wavefields (P) — denoted by solid lines — will be reflected via the reflectivity operator **R** and forward scattered via differential transmission operator δ**T**. The total wavefield leaving the gridpoint — including its scattering effects, denoted by the dashed lines — is called Q. (b) After propagation with operator **W**, wavefield Q, including the scattering δS of the current depth level, becomes the incident field P at the next depth level. (c) The full-wavefield modeling (FWMod) involves iterative, recursive downgoing and upgoing propagation of the wavefields, while each time updating the secondary scattering δS in each gridpoint. Note that, in this way, internal multiples and transmission effects are included.

propagates downward via wavefield propagation operator $\mathbf{W}^+(z_n, z_{n-1})$ or upward with $\mathbf{W}^-(z_{n-1}, z_n)$. All operators are defined in the space-fequency domain (see Berkhout, 1982). In Figures 1a and 1b, the wavefield relationships are explained (see Berkhout, 2014a for details). Note that $\delta\mathbf{T}^{\pm}(z_n, z_n)$ is the differential transmission in the down/up direction, where the full transmission operator $\mathbf{T}^{\pm}(z_n, z_n) = \mathbf{I} + \delta\mathbf{T}^{\pm}(z_n, z_n)$. Note also that in situations where wave conversion can be neglected, we may write $\delta\mathbf{T}^{+} = \mathbf{R}^{\cup}$ and $\delta\mathbf{T}^{-} = \mathbf{R}^{\cap}$, thus eliminating two unknowns in the equations.

The full-wavefield modeling can be formulated starting from the downgoing source field $\vec{S}_j^{+}(z_0)$ at the surface (z_0) from physical experiment (i.e., shot) number j (Berkhout, 2014a), as shown in Figure 1c:

(a) moving down ($m=1,2,\ldots..M$)

$$\vec{P}_j^{+}(z_m, z_0) = \mathbf{W}^{+}(z_m, z_0)\vec{S}_j^{+}(z_0) + \sum_{n=0}^{m-1}\mathbf{W}^{+}(z_m, z_n)\,\delta\vec{S}_j^{+}(z_n, z_0), \quad (1)$$

(b) moving up ($m=M-1,M-2,\ldots\ldots..0$)

$$\vec{P}_j^{-}(z_m; z_0) = \sum_{n=m+1}^{M}\mathbf{W}^{-}(z_m, z_n)\,\delta\vec{S}_j^{-}(z_n; z_0), \quad (2)$$

where vectors $\delta\vec{S}_j^{\pm}$ represent the *two-way* secondary sources in the inhomogeneous gridpoints at depth level z_n (see also Figures 1a and 1b).

By recursively applying equations 1 and 2, more orders of scattering are included in the wavefield modeling, thereby making the up/downgoing wavefield more complete. In the first round trip, only primaries are modeled (without transmission effects); in the second round trip, first-order multiples are included, and transmission effects become more accurate, etc. Note that such a recursive modeling scheme can be considered as a generalization of the so-called Bremmer series, which was originally defined for horizontally stratified media and plane wave propagation (Bremmer, 1951).

Finally, the observed data at the surface can be modeled by equation 2 by taking $z_m = z_0$ (see Figure 1c), assuming that we do not consider reflections from $z > z_M$ and that all original sources are at the surface. If the velocity model is known, an inversion process can be set up that updates the scattering operators ($\mathbf{R}^{\cup}$, $\mathbf{R}^{\cap}$), acting as convolutional operators in each gridpoint, such that the forward-modeled shot records from equation 2 match the observed data $\vec{P}_{obs,j}^{-}(z_0; z_0)$ — i.e., objective function

$$J(\mathbf{R}^{\cup}, \mathbf{R}^{\cap}) = \sum_j\sum_{\omega}||\vec{P}_{obs,j}^{-}(z_0; z_0) - \sum_{n=1}^{M}\mathbf{W}^{-}(z_0, z_n)\,\delta\vec{S}_j^{-}(z_n; z_0)||^2 \quad (3)$$

is minimized. This process is referred to as full-wavefield migration (FWM) (Berkhout, 2012; 2014b). Note that the "observed" data represents the upgoing wavefield at the surface, without any direct wave. Also note that, depending on the chosen coordinate system, diving waves may not be included. (See more on this in the discussion section.)

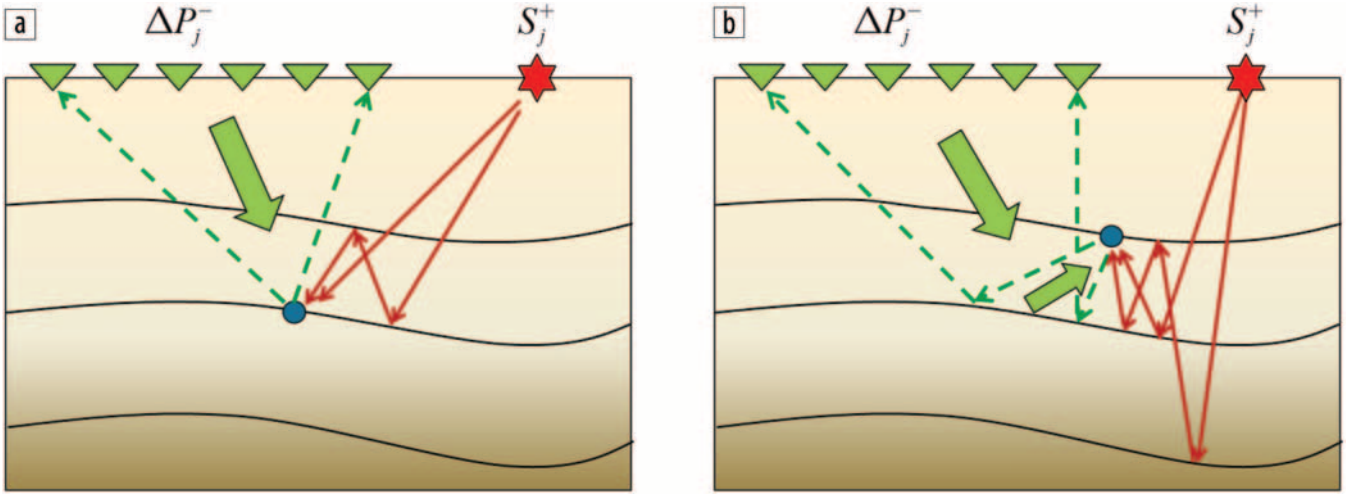

Figure 2. Reflectivity operators **R** are updated by combining wavefields in opposite directions. (a) Reflectivity operators **R** can be updated by combining the forward modeled, downgoing wavefield with the back-propagated residual data. (b) Reflectivity operators **R** can be updated by taking the back-propagated (residual) measured wavefield, reflecting it against the estimated boundaries and further back-propagating it upward, followed by deconvolution with the forward-modeled upgoing wavefield.

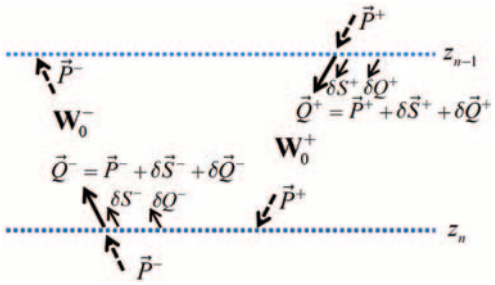

Figure 3. In joint migration inversion, the propagation operators are also considered unknowns in the update process. This can be implemented in the full-wavefield modeling by adding an additional scattering term δQ at each gridpoint that compensates for the local propagation error, while all wavefields propagate in the background medium, described by $\mathbf{W}_0$. If the background propagation operators are updated, then δQ becomes zero.

A key element in the minimization process is the updating of the scattering operators by combining, at each depth level, the back-propagated residual wavefield $\Delta\vec{P} = \vec{P}^-_{obs,j} - \vec{P}^-_j$ with the forward-modeled wavefield in the opposite direction via a suitable imaging condition. In Figures 2a and 2b, two options are given for combining wavefields in opposite directions, yielding updates for $\mathbf{R}^{\cup}$ and $\mathbf{R}^{\cap}$, respectively. Note that FWM, thus, can be used to separately update reflectivity from below, which is very useful in situations where reflections from above do not reach certain areas (Davydenko and Verschuur, 2013).

In JMI, we make velocity estimation part of the FWM process. The algorithm of JMI takes into account that for erroneous propagation velocities the propagation operators $\mathbf{W}^{\pm}$ are in error, causing phase errors. This is particularly true when including multiple scattering. If we represent the background or erroneous operators by $\mathbf{W}_0^{\pm}$, then we may write for the correct operators $\mathbf{W}^{\pm} = \mathbf{W}_0^{\pm} + \Delta\mathbf{W}^{\pm}$ or $\mathbf{W}^{\pm} = \mathbf{W}_0^{\pm}[\mathbf{I} + \delta\mathbf{W}^{\pm}]$. The initial propagation operators $\mathbf{W}_0^{\pm}$ are determined by the user-specified velocity distribution. Actually it means that all propagation can be described in the background model, provided that besides the *physical* scattering ($\delta\vec{S}_j^-$), *virtual* scattering ($\delta\vec{Q}_j^- = \delta\mathbf{W}^-\vec{Q}^-$) is also included, where the latter corrects for the propagation errors inside each layer (z_{n-1}, z_n), as illustrated in Figure 3. For more theoretical details, see Berkhout (2014c). Note that wavefield $\vec{Q}^{\pm}$ is defined as the wavefield leaving a depth level, including its scattering effect (see Figure 1a) . Thus, the full-wavefield modeling equations 1 and 2 in this situation become:

(a) moving down ($m=1,2,\ldots..M$)

$$\vec{P}_j^+(z_m,z_0) = \mathbf{W}_0^+(z_m,z_0)\,\vec{S}_j^+(z_0) + \sum_{n=0}^{m-1}\mathbf{W}^+(z_m,z_n)\left[\delta\vec{S}_j^+(z_n,z_0) + \delta\vec{Q}_j^+(z_n,z_0)\right], \quad (4)$$

(b) moving up ($m=M-1,M-2,\ldots\ldots\ldots0$)

$$\vec{P}_j^-(z_m;z_0) = \sum_{n=m+1}^{M}\mathbf{W}_0^-(z_m,z_n)\left[\delta\vec{S}_j^-(z_n;z_0) + \delta\vec{Q}_j^-(z_n;z_0)\right]. \quad (5)$$

JMI actually refers to the inversion process, where the forward-modeled data is compared with the observed data and aims at minimizing objective function:

$$J(\mathbf{R}^{\cup},\mathbf{R}^{\cap},\delta\mathbf{W}^+,\delta\mathbf{W}^-) = \sum_j\sum_{\omega}\left|\left|\vec{P}^-_{obs,j}(z_0;z_0) - \sum_{n=1}^{M}\mathbf{W}_0^-(z_0,z_n)\left[\delta\vec{S}_j^-(z_n;z_0) + \delta\vec{Q}_j^-(z_n;z_0)\right]\right|\right|^2, \quad (6)$$

where the unknowns are now both the reflectivity operators ($\mathbf{R}^{\cup}$, $\mathbf{R}^{\cap}$) as well as the differential propagation operators ($\delta\mathbf{W}^-$, $\delta\mathbf{W}^+$). Note that between two depth levels $\delta\mathbf{W}^-$ and $\delta\mathbf{W}^+$ are transposed versions of each other, so in fact only one $\delta\mathbf{W}$ needs to be estimated.

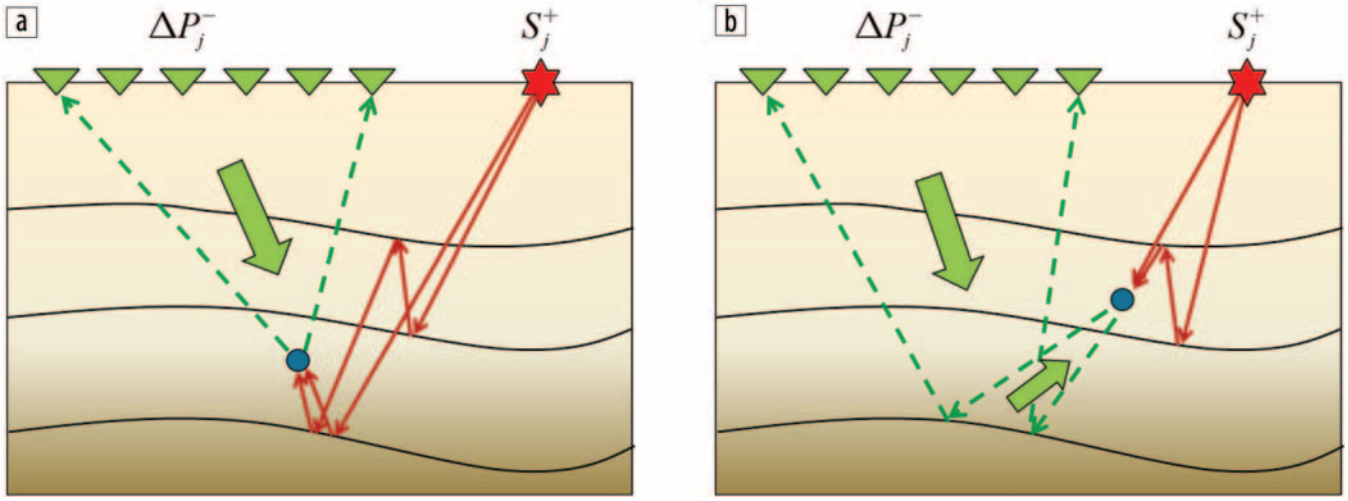

Figure 4. Propagation operators **W** are updated by combining wavefields in the same direction. (a) Upward propagation operators $\mathbf{W}^-$ can be updated by combining the forward modeled, upgoing wavefield with the back-propagated residual data. (b) Downward propagation operators $\mathbf{W}^+$ can be updated by taking the back-propagated residual wavefield, reflecting it against the estimated boundaries and further back-propagating it upward, followed by deconvolution with the forward-modeled downgoing wavefield.

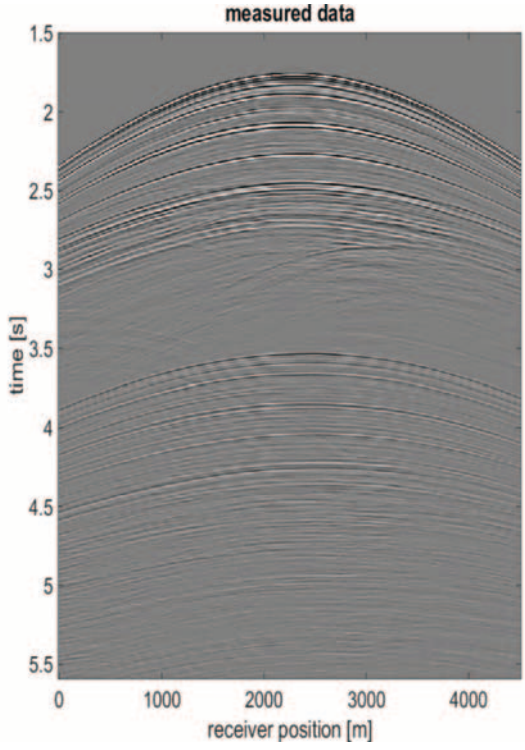

Figure 5. Example shot record from the 2D field data set from the Vøring area, offshore Norway.

For the updating of the propagation operators, again the residual wavefield at the surface is used, but now the gradients for the propagation update are obtained by combining wavefields that propagate in the same direction (see Figure 4).

The JMI algorithm can be carried out using two strategies with respect to the propagation errors. In the first option, the user-specified propagation operators ($\mathbf{W}_0^{\pm}$) are not updated, and the virtual scattering vectors ($\delta\mathbf{W}^{\pm}\bar{Q}_j^{\pm}$) are estimated to update the wavefields. This has the advantage that, in each iteration, the propagation operators are the same and can be accurately computed and stored in a table. The extra complexity is assigned to the hybrid secondary source vectors ($\delta\vec{S}^{\pm} + \delta\vec{Q}^{\pm}$). In the second option, the physical scattering vector ($\delta S^{\pm}$) is used only (similar to FWM), and the differential propagation operators ($\delta\mathbf{W}^{\pm}$) are used to update the propagation operators in each iteration (from $\mathbf{W}_0^{\pm}$ to $\mathbf{W}^{\pm}$). This has the advantage that $\delta\mathbf{W}^{\pm}$ becomes gradually smaller during the iteration. Moreover, in the second option, the update of $\delta\mathbf{W}^{\pm}$ can be linked immediately to a velocity update in the medium. This implementation was extensively used in the examples given by Staal (2015) and also in this paper. Optionally, $\delta\mathbf{W}^{\pm}$ can also be described with a few anisotropic parameters (Alshuhail et al., 2014).

Field data example of joint migration inversion

The JMI process is illustrated on a 2D field data set from the North Sea, in the Vøring area, offshore Norway. Statoil has provided the data. For this example, a subset is taken over a lateral extent of 4400 m, where sources and receivers are sampled at 25 m. Using near-offset interpolation and applying reciprocity, a fixed-spread data set of 181 × 181 traces is obtained as input, although only half the number of sources is actually used in the JMI process. The direct wave has been removed, and receiver deghosting was applied. The wavelet is estimated from the surface-related multiples using the so-called estimation of primaries by sparse inversion (EPSI) process (van Groenestijn and Verschuur, 2009). For this experiment, frequencies between 5 and 45 Hz have been used. Figure 5 shows one shot record from this pre-processed data set. In Figure 6, the results of the JMI process are shown, where Figures 6a and 6b show the initial reflectivity model (which is zero) and the initial velocity model, respectively. As the initial velocity model, a simple 1D velocity function has been chosen. Note that the image after JMI (Figure 6c) looks well focused, and the velocity field from JMI (Figure 6d) has clearly been updated, including lateral variations. Note the high-velocity layer that has been included in the middle part between 1700 and 2000 m depth. To verify the quality of the velocity model, angle

gathers are shown in Figures 7a and 7b before and after JMI velocity updating, respectively. Note the flattening of these gathers in Figure 7b. Of course, if velocities are estimated via the JMI process, such that the forward-modeled data correspond to the measured data, then image gathers are expected to be flat.

Robustness of the JMI process

One of the key features of the JMI process is that the two separate sets of unknowns — reflectivity and propagation velocity/operators — have decoupled effects on the data; the reflectivity is determined by the amplitude of reflection events, while the propagation effects are explained by their arrival times. This means that the method has freedom to create seismic events from whichever reflectivity and velocity model combination fits the data. Thus, during inversion, this could be a nonphysical realization — e.g., a homogeneous velocity that still has a large reflectivity at some depth. With typical FWI applications, using some form of finite difference modeling, such situation cannot be mimicked, as reflectivity is embedded in the velocity model. This also means that if the velocity is very wrong in the beginning of the JMI process, a reflectivity will be estimated at the wrong depth such that its modeled reflection events are still not too far from the observed seismic reflection data. For a simple situation of one reflector with a homogeneous overburden, this is schematically illustrated in Figure 8. Note that independent of the velocity error, the reflectivity information will readjust itself in depth to maximize the overlap of the modeled with the measured response. As a result, the JMI process will be able to overcome larger velocity errors than will traditional FWI concepts. Note that we help the *convergence speed* by employing a multiscale strategy: starting the JMI process with, e.g., 5–10 Hz, then using that result as input for a 5–20 Hz JMI process, etc.

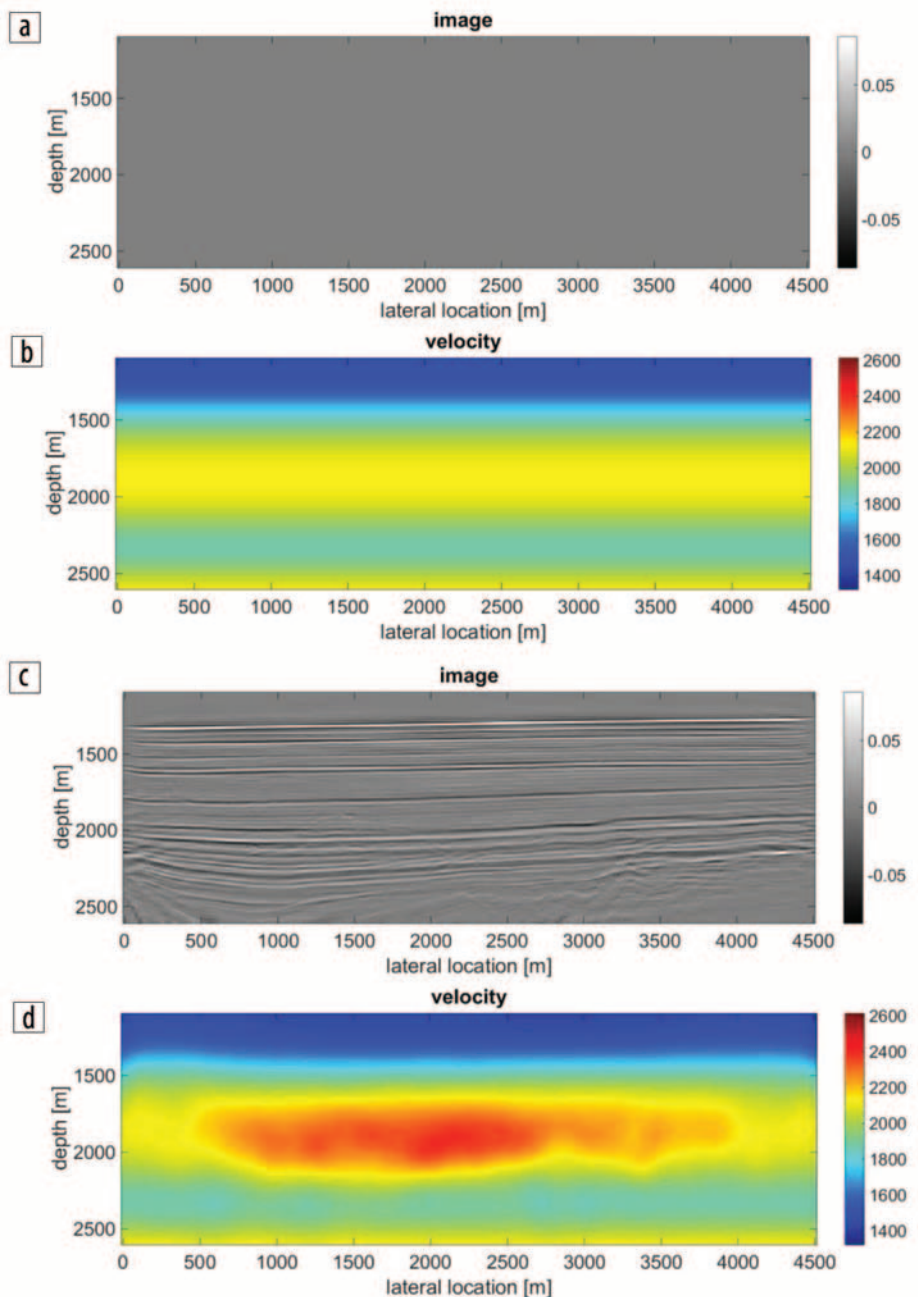

Figure 6. JMI results for the 2D field data. (a) Initial reflectivity model. (b) Initial velocity model based on a simple 1.5D profile. (c) Estimated JMI reflectivity. (d) Estimated JMI velocity model.

To illustrate this robustness aspect, a simple example based on a true velocity and density model from borehole data is shown in Figure 9. The input data is shown in Figure 9a and has a bandwidth of 5–80 Hz, whereas Figures 9b–9d visualize the output of JMI (velocity model and reflectivity as a function of depth) for three very different initial velocity models. For example, the first initial model has an average traveltime error in the medium of 100 ms. The results confirm that JMI automatically minimizes the errors in the user-specified velocity model, thus avoiding the notorious loop-skipping problem. The main effect of having a good initial model is efficiency, achieving the final result in less iterations.

Utilization of multiples

For the full-wavefield migration (FWM) process it already has been reported that multiples can contribute to the imaging process, both surface as well as internal multiples (Davydenko and Verschuur, 2013; Berkhout 2014b; Verschuur and Berkhout, 2015). This is especially true when the acquisition geometry is sparse or incomplete. Illumination shadow zones or surface obstruction areas may prevent some parts of the subsurface from being illuminated from enough different directions to provide

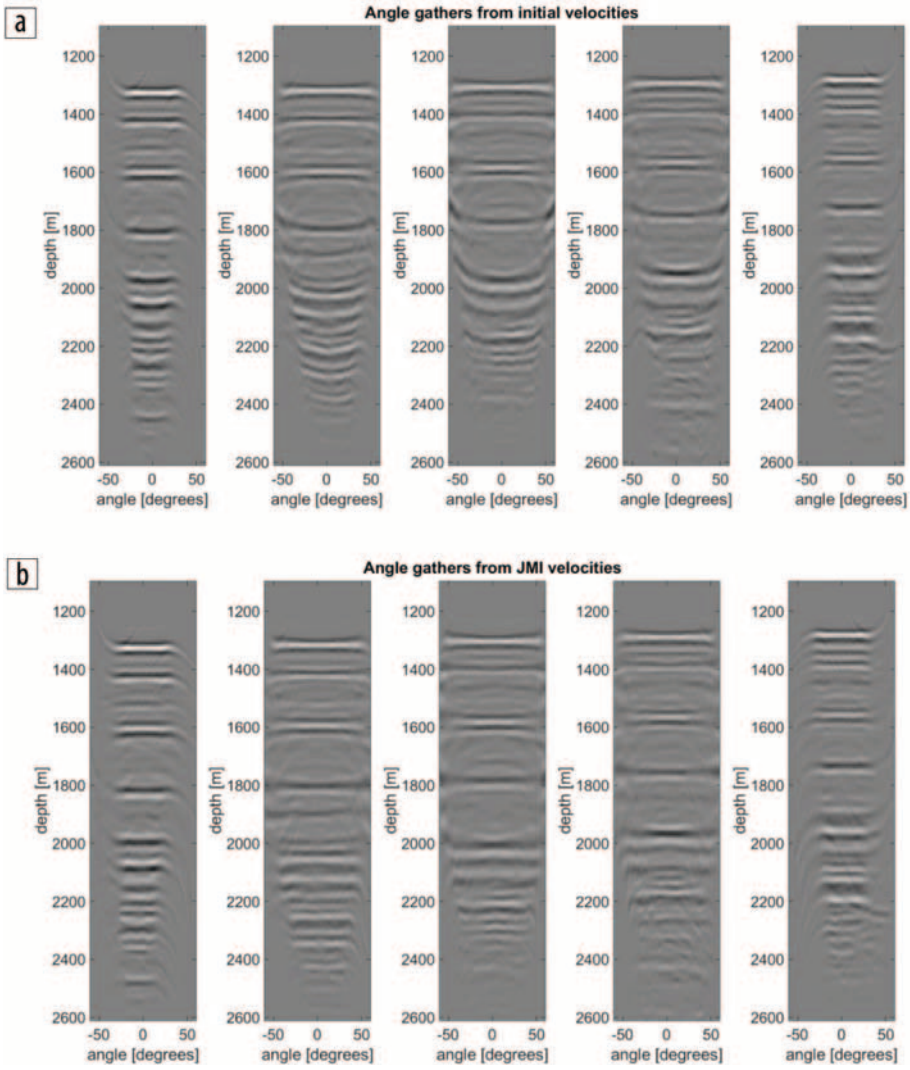

Figure 7. Quality control of the velocity estimation via traditional PSDM angle-domain image gathers. (a) Angle gathers calculated from the initial velocity model. (b) Angle gathers using the JMI velocity model.

good velocity estimates. In these cases, the added value of multiple scattering can be crucial to determine the velocity model and, thereby, to create reliable imaging results. Furthermore, it can be noted that the more complex the subsurface, the more omnidirectional the illumination by different multiples from different sources will be, and the more the velocity information can be extracted in an unambiguous manner.

We illustrate this feature in the model of Figure 10a (reflectivity) and Figure 10d (velocity) using data with a bandwidth of 2–30 Hz. Diffractors of 20 m vertical size have been included to better visualize the focusing quality. We assume that, during acquisition, sources could not be positioned in the middle part of the model such that this area will be poorly illuminated, as indicated by the red stars. Applying the JMI process, starting with a zero reflectivity and the initial model shown in Figure 10e, but excluding the multiples in the forward-modeling process, yields the image result shown in Figure 10b. Note that the starting model has been chosen too low in the area with poor illumination, yielding a nonideal starting situation. Although the left and right parts of the final image are quite well retrieved, the middle part is not properly resolved. By switching on the multiples in the modeling, the observed multiples are utilized. They considerably improve both the image (Figure 10c) and the velocity model (Figure 10f) in the central part, where, e.g., the diffractors are better focused and better imaged. Also note the improved focusing of the deepest reflector: illumination *and* velocity updating by multiples!

Elastic reflectivity estimation via JMI-res

Because JMI updates the background velocity model and finally retrieves the reflectivity operators that explain the measured data, these reflectivity operators by definition contain true elastic, angle-dependent PP reflection information. From these operators — via localized elastic inversion — the elastic properties at reservoir scale can be extracted.

This aspect is shown in Figure 11, in which a horizontally layered subsurface model is considered, denoted by the model shown in Figure 11a. Although only the P-wave velocities are shown, the model is full elastic, with density and S-wave velocities varying across these reflectors as well. The shallow, high-velocity layer produces a relatively strong internal multiple that masks the deepest primary reflection. Although stylized in this example, this is a typical situation observed, for example, in the Middle East. Figure 11b shows the observed data at the surface, which has been generated by full elastic modeling. The JMI process is used with P-wave velocity and elastic reflectivity as the parameters. Thus, only PP-reflections are predicted. Note that converted waves will not fit our forward model as we intentionally used somewhat higher initial velocities. Figure 11a shows the true velocity model in blue and the initial, smooth velocities in black. After updating, the final P-wave velocity model is given in red. Figure 11c shows the estimated reflections, and Figure11d shows the residual data. Note that only converted waves are visible here. After the JMI process, we analyze the estimated reflectivity of the deepest reflector, indicated by the red arrow in Figure 11b. After transforming the reflectivity information to the linear Radon domain and extracting the values at the target depth, we obtain the result shown in Figure 11f. As a comparison, Figure 11e displays the true angle-dependent reflectivity information in the linear Radon domain. Note that the resemblance is quite good, and the absolute amplitude is correctly retrieved. Note that the interference of the internal multiple is removed during the JMI process, as this multiple is explained by the estimated reflections in the overburden. As a comparison, we show the reflectivity information obtained at the target reflector for the case the internal multiple generation is

switched off in JMI, yielding the distorted result in Figure 11g. Thus, JMI preserves all important elastic reflectivity information, despite multiple interference, while only P-wave propagation was considered in the overburden. This emphasizes the advantage of using wavefield operators.

Final remarks and conclusions

At the moment, a discussion is taking place in the industry on the value of multiples in seismic imaging and inversion: are they signal or are they better removed in advance as "noise"? In case the acquisition geometry would be dense in all spatial dimensions and there would be no noise in the data, primaries will provide enough information to solve the inverse problem (Berkhout, 2016). However, both requirements are never met in practice, and, especially in cases of poor sampling in one or more spatial dimensions, the use of multiples will be indispensable in order to maximize the information from our seismic data. For the case of surface multiples, this has already been shown by various authors (see, e.g., Verschuur and Berkhout, 2011; Lu et al., 2013). Maybe the largest uplift is expected from borehole seismic data (Soni and Verschuur, 2014). However, it was also shown that the added effect of surface multiples decreases with imaging depth. On the other hand, internal multiples, with at least three reflection points within the subsurface, can have very different illumination paths compared to primaries. Therefore, it is expected that internal multiples will add value to deep areas and to imaging complex areas, such as salt layers or gas clouds.

Many aspects and extensions to the described JMI algorithm are currently investigated. First of all, we did not yet discuss additional constraints that can be brought in the objective function as given by equation 6. Options are sparseness in reflectivity, minimum total variation to velocity, and a soft coupling between velocity and reflectivity when the final inversion result is approached. Research in this area is ongoing (Maciel et al., 2015). Such constraints are especially helpful in time-lapse monitoring situations, for which JMI is very well suited (Qu and Verschuur, 2016). In the latter approach, multiple vintages of seismic data measured with different acquisition geometries are inverted such that the differences in the image and velocities are highlighted.

One issue for further research is the proper handling of horizontal scattering, duplex, and turning waves. Because the current implementation of the FWMod process prefers waves that propagate in the up/down direction, extensions to properly handling horizontal propagation and scattering need to be made. Some first steps have already been

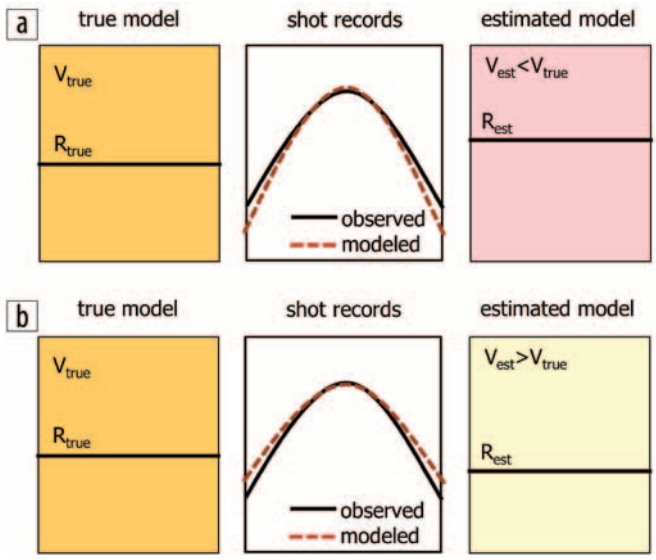

Figure 8. Robustness of the JMI process by using separate velocity and reflectivity parameters: when the estimated velocity is too low (a) the reflector is estimated more shallow such that the modeled shot record still overlaps with the true model and cycle-skip effects are suppressed. Similarly, in case of a too high velocity, (b) the estimated reflector will be positioned deeper in order to maximally match the observed data.

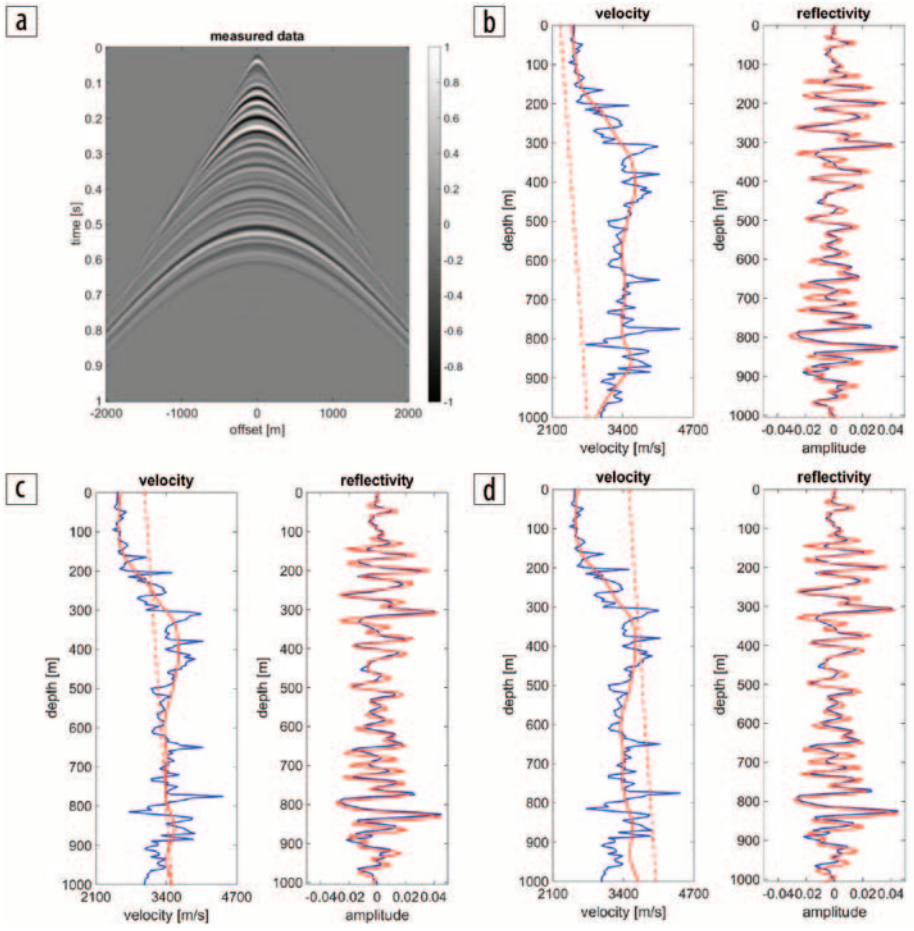

Figure 9. Demonstration of robustness of JMI with respect to the starting model. (a) Input data to be inverted. (b)–(d) JMI inversion results for three quite different starting models. The dashed red lines represent the initial velocity model, the solid red lines represent the estimated velocities/reflectivities, and the blue lines represent the true values (for which the input data is shown in [a]).

successful in imaging steep structures (Davydenko et al., 2014). A hybrid solution of JMI with FWI methods is an interesting option, where FWI takes care of the turning waves and JMI considers the reflection energy.

Another extension that needs further investigation is the inclusion of converted waves. This can be achieved by also including converted waves, via PS reflectivity operators and S-wave velocity propagators, as described by Berkhout (2014a).

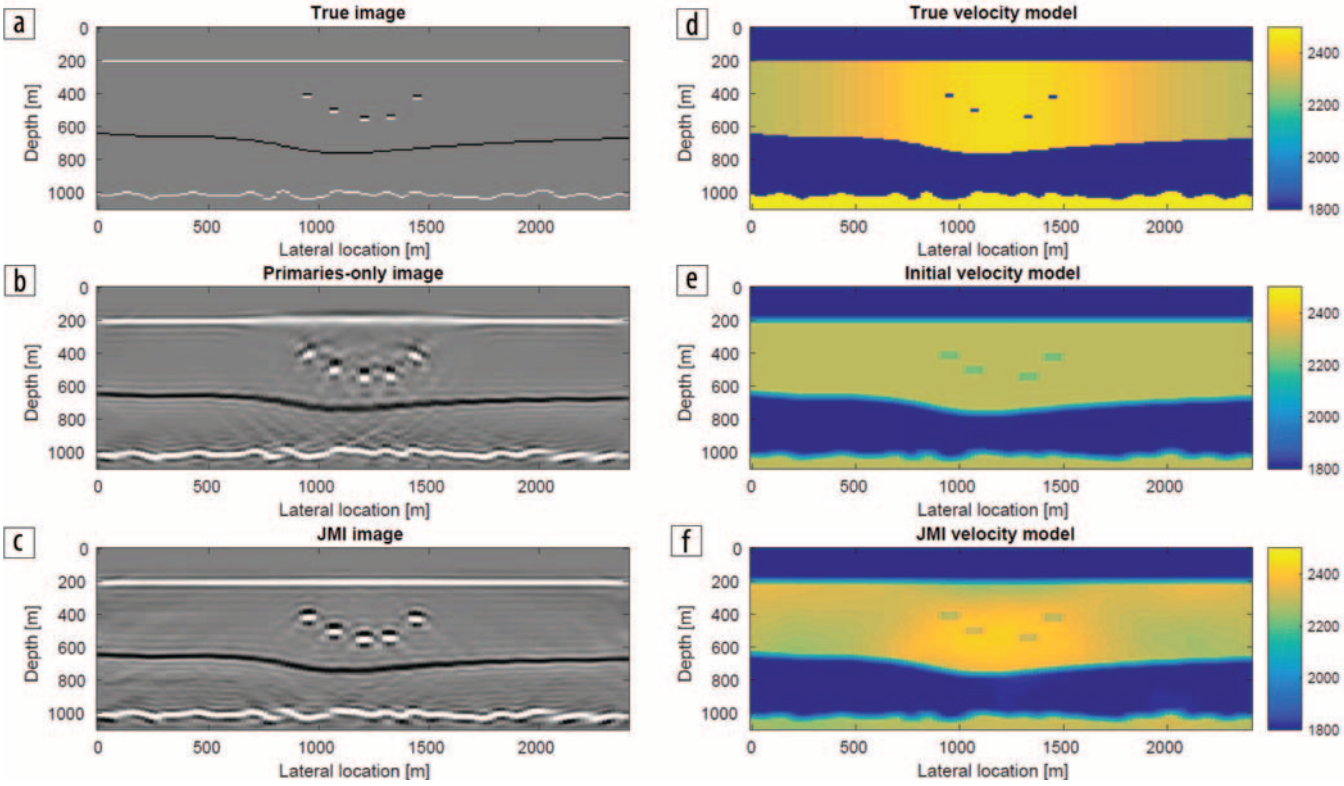

Figure 10. Contribution of multiples to both velocity update and reflectivity estimation. The source locations are indicated with the red stars, receivers are positioned along the full extent of the model. (a) True reflectivity model. (b) Estimated reflectivity after primaries-only JMI. (c) Estimated reflectivity after full-wavefield JMI. (d) True velocity model. (e) Initial velocity model with error mainly in the middle. (f) Estimated velocity model via full-wavefield JMI. Note that the velocity in the middle has been updated to get focused reflections via the multiples in (c).

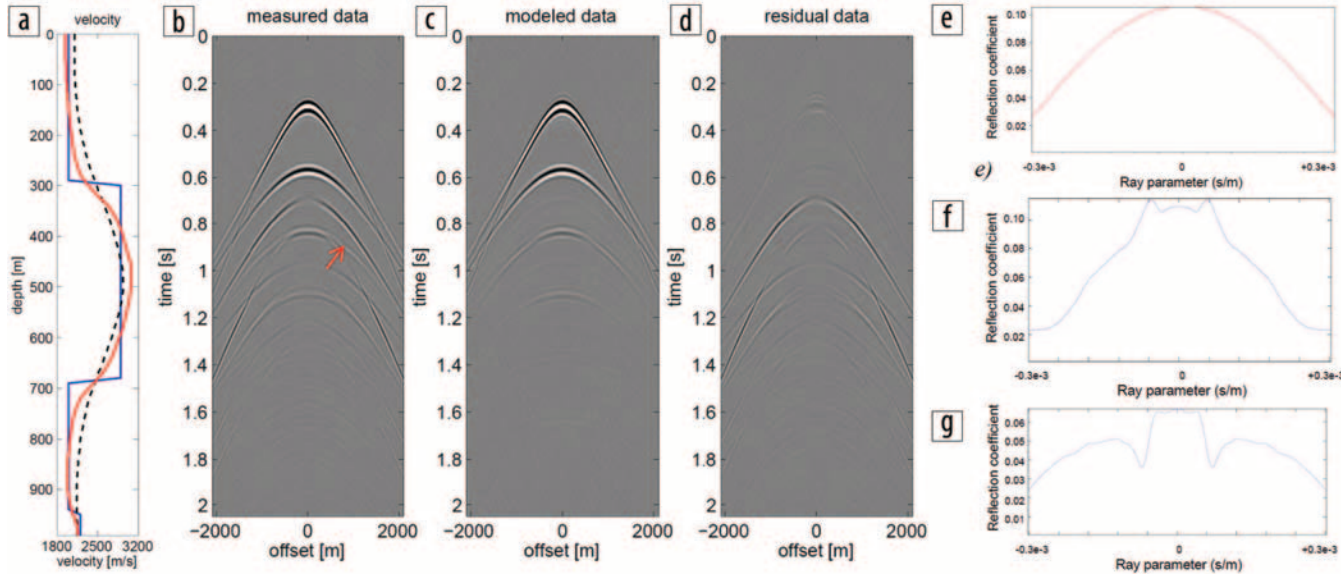

Figure 11. Estimation of full elastic reflectivity operators via JMI for an elastic subsurface model with high-velocity overburden layer. (a) True P-wave model (blue), initial P-wave model (black), and inverted P-wave velocities (red). (b) Observed shot record with the arrow indicating the target reflector that is overlaid with an internal multiple. (c) Forward-modeled data with inverted model. (d) Residual data, being mainly the converted reflections only. (e) True PP reflectivity information at the target reflector displayed in the linear Radon domain. (f) Estimated R_{PP} information for the target reflector using the full wavefield. Note the resemblance with the true shape. (g) Estimated R_{PP} after the primaries-only inversion. Note the wrong amplitude scale and angle-dependent behavior due to the internal multiple imprint.

Finally, as discussed before, a big advantage of JMI is that it does not require explicit velocity information during inversion, but it can directly estimate (differential) propagation operators **W** or δ**W**, without specifying any predefined velocity parameterization. This would facilitate the inclusion of any unknown anisotropy effect, as long as the modeled data matches the observed measurements. Translation from propagation operators into anisotropy parameters involves a separate step that is carried out after the JMI process. Note that such an approach is along the same lines as the so-called common-focus point (CFP) methodology (Berkhout, 1997), in which reflection-free propagation operators (W) were directly estimated from the data without parameterizing it via a velocity model. In addition, de CFP technology was based on our WRW model (Berkhout (1982).

All examples shown in this paper were on 2D data sets. Similar to traditional migration, the extension to 3D is straightforward as, technically speaking, it consists of wave-equation-based extrapolation and imaging steps, as shown by Davydenko and Verschuur (2015). One main issue in this process is the necessity to keep the up/downgoing wavefields for each shot experiment at each depth level in the subsurface. This can pose challenges to computer memory or require a smart IO strategy. In addition, the reflectivity operators **R** become two-dimensional convolution operators per frequency in each gridpoint, which poses some computational challenges. However, by using smart strategies — e.g., starting with scalar reflectivity (i.e. diagonal **R**-matrices) in the early iterations — this can be easily relieved.

In conclusion, the proposed JMI methodology has the major advantage that it is formulated in terms of reflectivity operators that are propagation-independent and propagation operators that are reflectivity-independent. This "orthogonality" property makes the inversion problem significantly more linear. A major advantage of our algorithm is (1) that multiples are utilized to improve both image and velocity accuracy, and (2) that both image and velocities are utilized to make a contribution in the nonlinear migration process. Hence, in joint migration inversion, multiples have a two-fold active role. TLE

Acknowledgments

The authors thank Statoil for providing the field data. Finally, the authors thank the members of the Delphi consortium for their financial support and the stimulating discussions during the meetings.

References

Alshuhail, A. A., X. R. Staal, and D. J. Verschuur, 2014, Incorporating anisotropy in joint migration inversion, 84th Annual International Meeting, SEG, Expanded abstracts, 415–419, http://dx.doi.org/10.1190/segam2014-0287.1

Berkhout, A. J., 1982, Seismic migration, imaging of acoustic energy by wavefield extrapolation — A. Theoretical aspects, 2nd ed.: Elsevier.

Berkhout, A. J., 1997, Pushing the limits of seismic imaging, Part II: Integration of prestack migration, velocity estimation, and AVO analysis: Geophysics, **62**, no. 3, 954–969, http://dx.doi.org/10.1190/1.1444202.

Berkhout, A. J., 2012, Combining full wavefield migration and full waveform inversion, a glance into the future of seismic imaging: Geophysics, **77**, S43–S50, http://dx.doi.org/10.1190/geo2011-0148.1.

Berkhout, A.J., 2014a-c, Review paper: An outlook on the future of seismic imaging, Part I–III: Geophysical Prospecting, **62**, no. 5, 911–971, http://dx.doi.org/10.1111/1365-2478.12161.

Berkhout, A. J., 2016, Utilization of multiple scattering: the next big step forward in seismic imaging: Geophysical Prospecting, **64**, online publication,1–40, http://dx.doi.org/10.1111/1365-2478.12395.

Biondi, B., and A. Almomin, 2013, Tomographic full-waveform inversion (TFWI) by combining FWI and wave-equation migration velocity analysis: The Leading Edge, **32**, no. 9, 1074–1080, http://dx.doi.org/10.1190/tle32091074.1.

Bremmer, H., 1951, The WKB approximation as the first term of a geometric-optical series: Communications on Pure and Applied Mathematics, **4**, no. 1, 105–115, http://dx.doi.org/10.1002/cpa.3160040111.

Chavent, G., F. Clément, and S. Gómez, 1994, Automatic determination of velocities via migration-based traveltime waveform inversion: A synthetic data example: 64th Annual International Meeting, SEG, Expanded Abstracts, 1179–1182, http://dx.doi.org/10.1190/1.1822731.

Clément, F., and G. Chavent, 1993, Waveform inversion through MBTI reformulation, in R. Kleinman, T. Angell, D. Colton, F. Santosa, and I. Stakgold, eds., Mathematical and numerical aspect of wave propagation: SIAM, 142–151.

Davydenko, M., and D. J. Verschuur, 2013, Full wavefield migration, using internal multiples for undershooting: 83rd Annual International Meeting, SEG, Expanded Abstracts, 3741–3745, http://dx.doi.org/10.1190/segam2013-1413.1.

Davydenko, M., D. J. Verschuur, and A. J. Berkhout, 2014, Omnidirectional extension of full wavefield migration: 76th Conference and Exhibition, EAGE, Extended Abstracts, Tu-G103-06, http://dx.doi.org/10.3997/2214-4609.20140777.

Davydenko, M., and D. J. Verschuur, 2015, Full wavefield migration for sparsely sampled 3D data: 85th Annual International Meeting, SEG, Expanded Abstracts, 4206–4210, http://dx.doi.org/10.1190/segam2015-5923846.1.

Fleury, C., and F. Perrone, 2012, Bi-objective optimization for the inversion of seismic reflection data: Combined FWI and MVA: 82nd Annual International Meeting, SEG, Expanded Abstracts, http://dx.doi.org/10.1190/segam2012-0797.1.

Krebs, J., C. C. Ober, T. M. Smith, J. R. Overfelt, S. S. Collis, G. J. von Winckel, B. G. van Bloemen Waanders, N. J. Downey, and D. Aldridge, 2016, Synthetic study of raw-data FWI applied to visco-TTI-elastic data: 86th Annual International Meeting, SEG, Expanded Abstracts, 1179–1183, http://dx.doi.org/10.1190/segam2016-13841891.1

Lu, S., N. D. Whitmore, H. LeGleut, and A. Long, 2013, 3D high-resolution imaging using separated wavefields: 75th Conference and Exhibition, EAGE, Extended abstracts, TH-08-09, http://dx.doi.org/10.3997/2214-4609.20130088.

Maciel, J. S., J. C. Costa, and D. J. Verschuur, 2015, Enhancing resolution in imaging-based velocity estimation using morphological operators: 85th Annual International Meeting, SEG, Expanded abstracts, 5228–5232, http://dx.doi.org/10.1190/segam2015-5900483.1.

Nemeth, T., C. Wu, and G. T. Schuster, 1999, Least-squares migration of incomplete reflection data: Geophysics, **64**, no. 1, 208–221, http://dx.doi.org/10.1190/1.1444517.

Operto, S., C. Ravaut, L. Improta, J. Virieux, A. Herrero, and P. Dell'Aversana, 2004, Quantitative imaging of complex structures from dense wide-aperture seismic data by multiscale traveltime and

waveform inversions: a case study: Geophysical Prospecting **52**, no. 6, 625–651, http://dx.doi.org/10.1111/j.1365-2478.2004.00452.x.
Plessix, R.-E., G. Baeten, J. W. de Maag, M. Klaassen, Z. Rujie, and T. Zhifei, 2010, Application of acoustic full waveform inversion to a low-frequency large-offset land data set: 80th Annual International Meeting, SEG, Expanded Abstracts, 930–934, http://dx.doi.org/10.1190/1.3513930.
Qu, S., and D. J. Verschuur, 2016, Simultaneous time-lapse imaging via joint migration and inversion: 78th Conference and Exhibition, EAGE, Extended Abstracts, Tu-LHR2-11.
Sava, P., and B. Biondi, 2004, Wave-equation migration velocity analysis. I. theory: Geophysical Prospecting, **52**, no. 6, 593–606, http://dx.doi.org/10.1111/j.1365-2478.2004.00447.x.
Soni, A. K., and D. J. Verschuur, 2014, Full-wavefield migration of vertical seismic profiling data: using all multiples to extend the illumination area: Geophysical Prospecting, **62**, no. 4, 740–759, http://dx.doi.org/10.1111/1365-2478.12130.
Staal, X. R., and D. J. Verschuur, 2012, Velocity estimation using internal multiples: 82nd Annual International Meeting, SEG, Expanded Abstracts, http://dx.doi.org/10.1190/segam2012-1580.1.
Staal, X. R., 2015, Combined imaging and velocity estimation by Joint Migration Inversion: Ph.D thesis, Delft University of Technology.
Stork, C., 1992, Reflection tomography in the postmigrated domain: Geophysics, **57**, no. 5, 680–692, http://dx.doi.org/10.1190/1.1443282.
Symes, W. W., 2008, Migration velocity analysis and waveform inversion: Geophysical Prospecting, **56**, no. 6, 765–790, http://dx.doi.org/10.1111/j.1365-2478.2008.00698.x.
Tarantola, A., 1984, Inversion of seismic reflection data in the acoustic approximation: Geophysics, **49**, no. 8, 1259–1266, http://dx.doi.org/10.1190/1.1441754.
van Groenestijn, G. J. A., and D. J. Verschuur, 2009, Estimating primaries by sparse inversion and application to near-offset data reconstruction: Geophysics, **74**, no. 3, A23–A28, http://dx.doi.org/10.1190/1.3111115.
Verschuur, D. J., and A. J. Berkhout, 2011, Seismic migration of blended shot records with surface-related multiple scattering: Geophysics, **76**, no. 1, A7–A13, http://dx.doi.org/10.1190/1.3521658.
Verschuur, D. J., and A. J. Berkhout, 2015, From removing to using multiples in closed-loop imaging: The Leading Edge, **34**, no. 7, 744–759, http://dx.doi.org/10.1190/tle34070744.1.
Virieux, J., and S. Operto, 2009, An overview of full-waveform inversion in exploration geophysics: Geophysics, **74**, no. 6, WCC1–WCC26, http://dx.doi.org/10.1190/1.3238367.
Wang, F., H. Chauris, D. Donno, and H. Calandra, 2013, Taking advantage of wave field decomposition in full waveform inversion: 75th Conference and Exhibition, EAGE, Extended Abstracts, Tu-0708, http://dx.doi.org/10.3997/2214-4609.20130415.
Wu, Z., and T. Alkhalifah, 2015, Simultaneous inversion of the background velocity and the perturbation in full-waveform inversion: Geophysics, **80**, no. 6, R317–R329, http://dx.doi.org/10.1190/geo2014-0365.1.
Zhou, H., L. Amundsen, and G. Zhang, 2012, Fundamental issues in full waveform inversion: 82nd Annual International Meeting, SEG, Expanded Abstracts, http://dx.doi.org/10.1190/segam2012-0878.1.